

# VLA-IAP: Training-Free Visual Token Pruning via Interaction Alignment for Vision-Language-Action Models

Jintao Cheng<sup>1</sup>, Haozhe Wang<sup>3</sup>, Weibin Li<sup>3</sup>, Gang Wang<sup>2</sup>, Yipu Zhang<sup>1</sup>, Xiaoyu Tang<sup>3</sup>, Jin Wu<sup>5</sup>, Xieyuanli Chen<sup>4</sup>, Yunhui Liu<sup>2</sup>, and Wei Zhang<sup>1\*</sup>

<sup>1</sup> The Hong Kong University of Science and Technology  
eeweiz@ust.hk

<sup>2</sup> The Chinese University of Hong Kong

<sup>3</sup> South China Normal University

<sup>4</sup> National University of Defense Technology

<sup>5</sup> University of Science and Technology Beijing

**Abstract.** Vision-Language-Action (VLA) models have rapidly advanced embodied intelligence, enabling robots to execute complex, instruction-driven tasks. However, as model capacity and visual context length grow, the inference cost of VLA systems becomes a major bottleneck for real-world deployment on resource-constrained platforms. Existing visual token pruning methods mainly rely on semantic saliency or simple temporal cues, overlooking the continuous physical interaction, a fundamental property of VLA tasks. Consequently, current approaches often prune visually sparse yet structurally critical regions that support manipulation, leading to unstable behavior during early task phases. To overcome this, we propose a shift toward an explicit Interaction-First paradigm. Our proposed **training-free** method, VLA-IAP (Interaction-Aligned Pruning), introduces a geometric prior mechanism to preserve structural anchors and a dynamic scheduling strategy that adapts pruning intensity based on semantic-motion alignment. This enables a conservative-to-aggressive transition, ensuring robustness during early uncertainty and efficiency once interaction is locked. Extensive experiments show that VLA-IAP achieves a **97.8% success rate** with a  $1.25\times$  **speedup** on the LIBERO benchmark, and up to  $1.54\times$  **speedup** while maintaining performance **comparable to the unpruned backbone**. Moreover, the method demonstrates superior and consistent performance across multiple model architectures and three different simulation environments, as well as a real robot platform, validating its strong generalization capability and practical applicability. Our project website is: VLA-IAP.com.

## 1 Introduction

Vision-Language-Action (VLA) models mark a paradigm shift in embodied intelligence. By integrating the reasoning power of Large Language Models (LLMs) with visual perception and action, these systems excel at executing complex instructions in unstructured environments. Foundation models like OpenVLA [12],

---

\* Corresponding author.

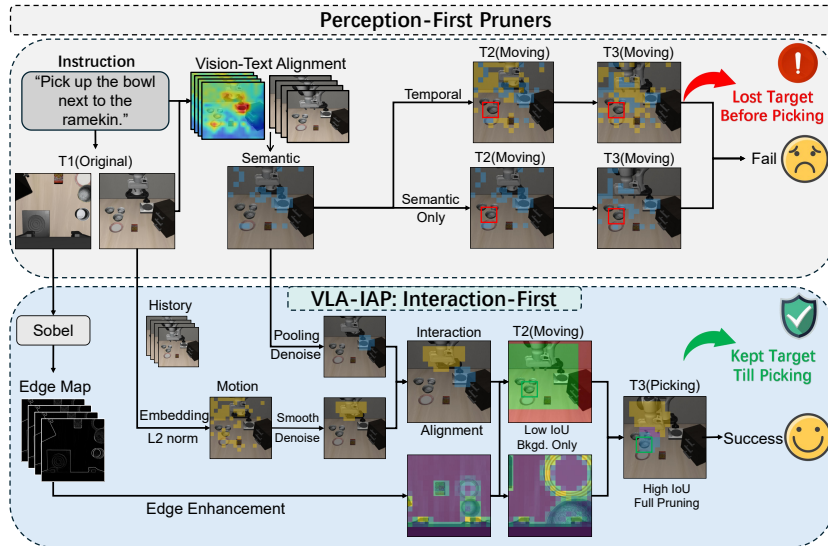


**Fig. 1. Comparison of Perception-First vs. Interaction-First token pruning paradigms.** Perception-First baselines (Top) prematurely lose the manipulation target due to early semantic misalignment—a vulnerability that simple temporal stacking Temporal branch fails to resolve without explicit interaction modeling. In contrast, our VLA-IAP (Bottom) shifts to an Interaction-First approach. By coupling geometric priors with an IoU-aware dynamic strategy—transitioning from conservative (background-only) to aggressive (full) pruning—VLA-IAP successfully preserves the physical target for precise execution.

RT-1 [3], and  $\pi_0$  [2] demonstrate that this end-to-end architecture generalizes well to unseen objects and tasks. Yet, this versatility comes at a steep computational cost. Processing long visual sequences creates significant latency, limiting inference to under 5 Hz, far from the required frequency for robust closed-loop robotic control. Since the LLM backbone dominates this latency [8,13], efficient visual token pruning has become a prerequisite for deploying these systems in the real world.

While visual compression has evolved from static semantics to dynamic strategies, current robotic pruning methods suffer from a critical blind spot. Most inherit a Perception-First bias from standard Vision-Language Models (VLMs), treating the goal of vision as semantic understanding rather than physical affordance discovery.

Early static approaches (e.g., FastV [5], SparseVLM [26], SP-VLA [14]) relied on attention to filter tokens based on instruction semantics. However, this passive approach is susceptible to early semantic misalignment. As illustrated in Fig. 1, target objects in the original phase (time =  $T_1$ ) are often off-center or obscured by clutter. Consequently, models tend to prioritize semantically salient backgrounds

while discarding regions that are visually sparse but dynamically essential for manipulation, such as smooth handles or transparent edges. This indicates an inherent limitation in visual encoders, where semantic appearance is prioritized over the geometric structures required for manipulation (Fig. 1, **Semantic Only** stage).

Later works (e.g., VLA-Cache [21], EfficientVLA [22], SpecPrune-VLA [19], VLA-ADP [17]) incorporated spatiotemporal and action cues to enable dynamic pruning regulation (Fig. 1, **Temporal** stage). While these approaches transition from static perception to dynamic regulation, their token selectors remain dependent on the model’s internal attention scores. This dependency creates a logical constraint: if the pre-trained model overlooks certain geometric details due to a lack of physical continuity, pruning based on its attention scores inherits and amplifies these errors. Consequently, this strategy fails to correct the model’s inherent lack of physical grounding.

In summary, existing pruning paradigms are limited by a passive perspective that neglects the physical constraints defining embodied vision. To address this issue, we propose VLA-IAP (**Interaction-Aligned Pruning**), a **training-free** method that shifts embodied visual compression toward an Explicit Interaction-First paradigm (illustrated in Fig. 1). Our design incorporates two key components to align token selection with the robot’s physical intent. First, we introduce a Geometric Prior Mechanism to preserve structural anchors independent of semantic attention. Second, we develop an Interaction-Aligned Dynamic Strategy that adjusts pruning intensity based on semantic-motion alignment. We measure this alignment using the Intersection over Union (IoU) between semantic and motion masks. In the early phase, where semantic focus diverges from physical motion (Low IoU), the system adopts a conservative approach to retain non-background information. As the task progresses, when semantic intent aligns with the arm’s physical motion (High IoU), the system triggers aggressive pruning. This logic transforms the pruning process from a passive filter into a mechanism that actively preserves geometric anchors and ensures operational safety. Based on the above design philosophy, the main contributions of this paper are summarized as follows:

1. We introduce a **Geometric Prior Mechanism** to rectify the inherent bias towards semantic appearance. By employing lightweight edge enhancement, this module explicitly extracts physical contours, ensuring that texture-poor but structurally critical interaction anchors are preserved. This fundamentally corrects the model’s tendency to focus on semantic-rich backgrounds while ignoring actionable geometric features.
2. We propose an **Interaction-Aligned Dynamic Strategy** coupling spatiotemporal priors with an adaptive safety mechanism. By leveraging a Semantic-Motion IoU metric to assess interaction lock, the system dynamically switches

between conservative and aggressive pruning modes, preventing premature token loss and ensuring robustness under extreme compression.

3. We validate VLA-IAP through rigorous evaluations across three simulation benchmarks and real-world robotic deployments. On the LIBERO [15] benchmark, it achieves a state-of-the-art 97.8% success rate with a  $1.25\times$  speedup, and sustains a  $1.54\times$  speedup without performance degradation compared to the unpruned baseline. Real-world experiments further confirm its practical viability, demonstrating up to a  $1.48\times$  inference acceleration while simultaneously improving the average manipulation success rate. Code will be publicly released.

## 2 Related Work

### 2.1 Vision-Language-Action Models

Vision-Language-Action (VLA) models integrate pre-trained vision-language models with robotic action prediction frameworks. RT-1 [3] implements discrete action spaces for robotic manipulation tasks using a transformer-based policy. Its extension RT-2 [27] demonstrates zero-shot generalization capabilities to novel objects and tasks through web-scale semantic reasoning. Recent works adopt continuous action representations:  $\pi_0$  [2] employs diffusion policies for precise motor control, while OpenVLA [12] integrates diverse robotic datasets for instruction-following tasks, including object manipulation and container handling. Subsequent work such as OpenVLA-OFT [11] introduces action chunking and parallel decoding to improve temporal consistency. Additionally, CogACT [13] introduces a componentized architecture with decoupled cognitive and action modules, utilizing diffusion transformers for action generation and demonstrating zero-shot generalization to novel objects and robotic platforms. These models process high-resolution multi-view inputs, using LLM backbones with 7B+ parameters [13], resulting in high inference latency that hinders real-time deployment on resource-constrained robotic platforms.

### 2.2 Visual Token Compression for VLA

Token compression techniques for VLA models have evolved from static frame-level strategies toward temporally aware designs. FastV[5] reduces intra-frame redundancy via saliency-guided token scoring, while SparseVLM[26] applies sparse attention to suppress visually redundant regions. To leverage temporal continuity in robotic tasks, VLA-Cache [21] proposed caching stable background tokens across frames. TEAM-VLA[23] introduced hierarchical token merging within observations, and SpecPrune-VLA [19] utilized spectral-domain analysis to retain action-critical visual features. However, existing methods primarily rely on static cues, neglecting dynamic temporal characteristics and object geometry. In contrast, our VLA-IAP leverages motion-aware spatiotemporal dynamics and geometric structures for pruning, achieving efficient inference while improving task success rates.

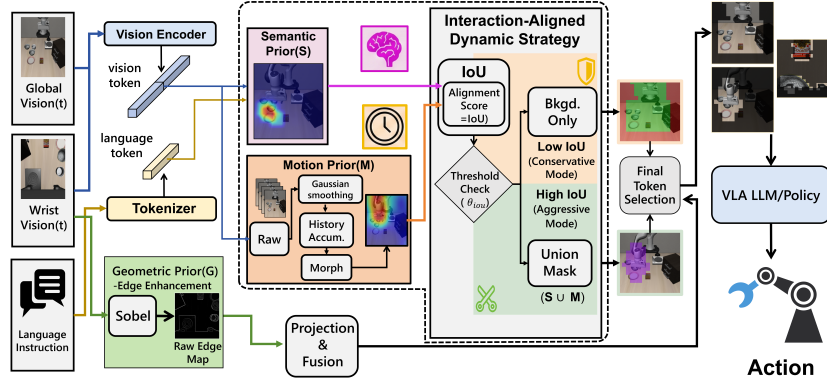


**Fig. 2. Overview of the proposed interaction-aligned dynamic strategy for vision–language action.** Given consecutive visual frames and a language instruction, a vision encoder extracts patch features, while three complementary priors are constructed: semantic prior  $S$ , motion prior  $M$  (via Gaussian modeling, history accumulation, and morphology), and geometric prior  $G$  (Sobel-based edge enhancement). The priors are projected and fused, and an IoU-based alignment score is computed to adaptively select background-only filtering or conservative/aggressive masking, producing a union mask ( $S \cup M$ ). After final token selection, the resulting visual tokens are fed into a VLA LLM/policy to generate the robot action.

### 3 Methodology

#### 3.1 Overview

In this paper, we propose the Interaction-Aligned Pruning (VLA-IAP) framework. The core of this framework is to break the Perception-First bottleneck prevalent in existing VLA pruning methods—namely, the over-reliance on the static attention weights of pre-trained Vision-Language Models (VLMs). Such reliance often causes models to prioritize semantic salience over physical affordances, inadvertently discarding geometric structures during compression that are visually sparse but critical for physical manipulation.

As illustrated in Fig. 2, VLA-IAP formulates visual sequence compression as a dynamic affordance extraction process. Once the vision encoder extracts the initial token sequence  $X^{vis}$ , the framework evaluates the physical importance of each token in parallel across three dimensions: Semantic Prior, Motion Prior, and Geometric Prior. Subsequently, our Interaction-Aligned Strategy identifies the manipulation state in real time by computing the spatial overlap (IoU) between semantic intent and physical motion. Based on this state, it dynamically switches between a Conservative and an Aggressive pruning mode, ultimately feeding the refined set of visual tokens into the LLM for action inference.

#### 3.2 Geometric Prior for Edge Enhancement

To directly extract and preserve the structural anchors required for physical manipulation, VLA-IAP incorporates an explicit Geometric Prior. Given an observation image  $I \in \mathbb{R}^{H \times W \times 3}$  at the current time step, the visual encoder maps

it into a dense visual token sequence  $X^{vis} \in \mathbb{R}^{N \times D}$ , where  $N = \frac{H}{P} \times \frac{W}{P}$  denotes the number of patches and  $P$  represents the patch size. To capture pure physical contours independent of semantic color information, we convert the original image to grayscale  $I_{gray}$  and apply a high-pass edge detection operator (Sobel) in the image space to extract pixel-level geometric gradients:

$$G_x = I_{gray} * K_x, \quad G_y = I_{gray} * K_y \quad (1)$$

where  $*$  denotes 2D convolution, and  $K_x, K_y \in \mathbb{R}^{3 \times 3}$  are directional convolution kernels. The edge strength magnitude  $\mathcal{G}(u, v)$  at pixel  $(u, v)$  is defined as:

$$\mathcal{G}(u, v) = \sqrt{G_x(u, v)^2 + G_y(u, v)^2} \quad (2)$$

To align with token-level multimodal features, we aggregate the pixel-level edge strength  $\mathcal{G}$  to the corresponding feature resolution. Let  $\mathcal{P}_i$  denote the original pixel region corresponding to the  $i$ -th token. Its geometric structure score  $E_i$  is calculated as the average response of edge strength within this region:

$$E_i = \frac{1}{|\mathcal{P}_i|} \sum_{(u,v) \in \mathcal{P}_i} \mathcal{G}(u, v), \quad i \in \{1, 2, \dots, N\} \quad (3)$$

Subsequently, all scores are normalized to  $[0, 1]$  to obtain the edge-enhanced prior vector  $\mathbf{E} = [\tilde{E}_1, \tilde{E}_2, \dots, \tilde{E}_N]$ . This normalized vector  $\mathbf{E}$  constitutes a physical Affordance map independent of the VLM semantic space. Specifically, a higher value of  $\tilde{E}_i$  indicates a stronger edge gradient, which corresponds to sharp geometric variations and clear object boundaries. In robotic manipulation, these structural contours are inherently the primary functional areas where physical interactions occur. Therefore, a larger  $\tilde{E}_i$  directly signifies a higher degree of physical affordance. By integrating this prior, VLA-IAP compels the system to assign high retention weights to tokens with high  $\tilde{E}_i$  but weak semantic attention. This effectively prevents critical manipulation boundaries from being misclassified as redundant background during compression.

### 3.3 Semantic-Motion Alignment Module

Guided by the Interaction-First paradigm, effective visual compression requires responding to both the semantic intent of language instructions and the dynamic feedback of physical scenes. This section details the construction of semantic and motion priors, followed by the interaction-aligned strategy that leverages their consistency for adaptive pruning.

**Semantic Prior.** In VLA architectures, semantic priors establish foundational intent alignment between language instructions and visual observations. Given dense visual features  $X^{vis} = \{\hat{x}_i\}_{i=1}^N$  and text instruction features  $\hat{e}_{text}$ , both processed with spatial centering and  $L_2$  normalization, we derive the initial cross-modal attention distribution by computing their dot-product similarity scaled by a temperature coefficient  $\tau = 0.01$ :

$$p_i = \frac{\exp((\hat{x}_i \cdot \hat{e}_{text})/\tau)}{\sum_{j=1}^N \exp((\hat{x}_j \cdot \hat{e}_{text})/\tau)} \quad (4)$$

To smooth local noise and enhance spatial connectivity, we apply spatial Average Pooling to the probability map  $p$ , followed by min-max normalization, directly mapping it to the final semantic saliency score  $\mathcal{S}_{sem} \in [0, 1]^N$ .  $\mathcal{S}_{sem}$  quantifies the static semantic matching degree between spatial regions and the manipulation instruction. As a baseline intent representation, it is fused and cross-verified with genuine physical feedback (motion priors) in subsequent dynamic strategies guided by the coefficient  $k$ .

**Motion Prior.** Existing dynamic pruning methods[19,17] typically rely on both first-order velocity signals in action space and visual attention scores to regulate pruning strategies. This design presents two limitations. First, action predictions are often unstable during early manipulation stages, and first-order velocity signals primarily represent macroscopic displacement, making them sensitive to linear trends such as camera panning or illumination changes. Second, the spatial assumptions inherent in attention mechanisms often result in fragmented response regions, lacking the connectivity required for physical interaction scopes.

To address this, VLA-IAP constructs a robust motion prior directly on visual features rather than relying on action space signals. Our design incorporates two key components: a second-order temporal difference to filter linear ego-motion noise, and spatial smoothing operations to ensure connectivity within interaction scopes. Specifically, we first quantify local motion changes by computing the magnitude of the second-order temporal difference across adjacent frames. Let the projected visual token sequence at time step  $t$  be denoted as  $X_t \in \mathbb{R}^{N \times D}$ . We compute:

$$d_{t,i} = \|X_{t,i} - 2X_{t-1,i} + X_{t-2,i}\|_2, \quad i \in \{1, 2, \dots, N\} \quad (5)$$

where  $\|\cdot\|_2$  denotes the  $L_2$  norm across the feature dimension. From a signal processing perspective, the second-order difference serves as a discrete approximation of acceleration in feature evolution. This effectively filters out linear background drift induced by smooth camera panning or gradual illumination changes, highlighting local regions where motion states change.

To ensure spatial continuity within the physical interaction scope, we reshape the 1D response  $d_t$  into a 2D spatial grid  $M_t$ . We explicitly introduce Morphological Closing and Gaussian Smoothing to enhance the connectivity of response regions. Additionally, we introduce a decay factor  $\gamma$  for History Accumulation to smooth noise in instantaneous detection:

$$H_t = (1 - \gamma)M_t + \gamma H_{t-1} \quad (6)$$

$$\tilde{M}_t = ((H_t \oplus K_{str}) \ominus K_{str}) * \mathcal{N}(0, \sigma^2) \quad (7)$$

where  $\oplus$  and  $\ominus$  denote morphological dilation and erosion operations, respectively,  $K_{str}$  is the structuring element,  $*$  represents 2D spatial convolution, and  $\mathcal{N}(0, \sigma^2)$  is the Gaussian smoothing filter with kernel radius  $\sigma$ . Finally,  $\tilde{M}_t$  is flattened back into a 1D sequence and normalized via min-max normalization to obtain the final temporal saliency score  $\mathcal{S}_{temp} \in [0, 1]^N$ . Through this mechanism,

the system obtains a purely kinematics-driven dynamic constraint, providing a reliable kinematic baseline for subsequent pruning.

**Interaction-Aligned Dynamic Strategy.** Building upon the preceding modules, the system has established multi-dimensional physical prior representations encompassing geometry, semantics, and motion. In this section, we leverage semantic and motion priors to achieve an Interaction Lock by quantifying the spatial consistency between operation intent and physical feedback, thereby enabling adaptive switching between Conservative and Aggressive pruning modes.

Specifically, we convert the derived semantic score  $\mathcal{S}_{sem}$  and motion score  $\mathcal{S}_{temp}$  into binary spatial masks using adaptive thresholds:

$$\mathcal{B}_{sem} = \mathbb{I}(\mathcal{S}_{sem} > \mu_{sem} + k \cdot \sigma_{sem}) \quad (8)$$

$$\mathcal{B}_{temp} = \mathbb{I}(\mathcal{S}_{temp} > \mu_{temp} + k \cdot \sigma_{temp}) \quad (9)$$

where  $\mu_*$  and  $\sigma_*$  denote the mean and standard deviation of the corresponding scores,  $k$  is a sensitivity coefficient, and  $\mathbb{I}(\cdot)$  is the indicator function. By computing the Intersection over Union  $\text{IoU}_t = \frac{|\mathcal{B}_{sem} \cap \mathcal{B}_{temp}|}{|\mathcal{B}_{sem} \cup \mathcal{B}_{temp}|}$ , VLA-IAP departs from traditional fixed-ratio truncation. Instead, it utilizes  $\text{IoU}_t$  as a gating signal to determine the token retention set  $\mathcal{K}_t$ , where  $\theta_{iou}$  denotes the threshold for switching between conservative and aggressive pruning modes:

*Conservative Mode (Exploration Phase,  $\text{IoU}_t \leq \theta_{iou}$ ):* The system employs a double-weak exclusion strategy. A region is classified as pure background only if both semantic and motion signals fall below the exclusion threshold (set by a negative coefficient  $k_{bg} < 0$ ). We introduce a background exclusion coefficient  $k_{bg} < 0$  to compute the joint background mask:

$$\mathcal{B}_{bg} = \mathbb{I}(\mathcal{S}_{sem} < \mu_{sem} + k_{bg}\sigma_{sem}) \wedge \mathbb{I}(\mathcal{S}_{temp} < \mu_{temp} + k_{bg}\sigma_{temp}) \quad (10)$$

The visual retention set is defined as  $\mathcal{K}_t = \{x_i \in X^{vis} \mid \mathcal{B}_{bg,i} = 0\}$ . The logical AND operation ensures robust retention, meaning tokens are preserved if either semantic intent or physical motion signals are strong. This design ensures that potential target regions and structural anchors are not irreversibly discarded before semantic-motion alignment is locked, thereby maintaining broad visual context recall.

*Aggressive Mode (Interaction Lock Phase,  $\text{IoU}_t > \theta_{iou}$ ):* Intent and physical feedback are highly aligned. We shrink the semantic mask towards the highest response center  $c^* = \arg \max(\mathcal{S}_{sem})$ , retaining the core semantic region  $\mathcal{B}_{sem}^{core} = \mathcal{B}_{sem} \wedge \mathbb{I}(\text{dist}(x_i, c^*) \leq r)$  within radius  $r$ . Subsequently, we take the union with the physical motion region to eliminate all static redundant background:

$$\mathcal{K}_t = \{x_i \in X^{vis} \mid (\mathcal{B}_{sem,i}^{core} \vee \mathcal{B}_{temp,i}) = 1\} \quad (11)$$

The Semantic-Motion Alignment module outputs the preliminary set of retained visual Tokens  $\mathcal{K}_t$  through adaptive mode switching:

$$\mathcal{K}_t = \begin{cases} \{x_i \in X^{vis} \mid \mathcal{B}_{bg,i} = 0\}, & \text{if } \text{IoU}_t \leq \theta_{iou} \\ \{x_i \in X^{vis} \mid (\mathcal{B}_{sem,i}^{core} \vee \mathcal{B}_{temp,i}) = 1\}, & \text{if } \text{IoU}_t > \theta_{iou} \end{cases} \quad (12)$$

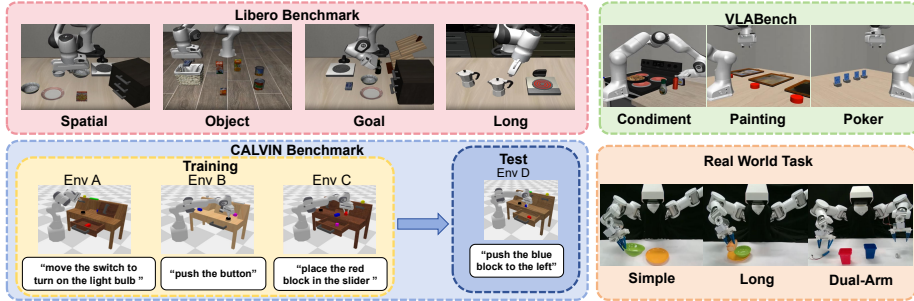


**Fig. 3.** Overview of the evaluation benchmarks and tasks. We evaluate on simulated benchmarks including Libero, VLABench, and CALVIN ABC-D, as well as real-world tasks covering simple, long-horizon, and dual-arm manipulation.

### 3.4 Final Visual Token Selection

Geometric priors are incorporated at this stage. This explicit fusion ensures that the structural integrity of physical operation boundaries is preserved, even under extreme compression. We compute a comprehensive priority score for each token:

$$\text{Score}_i = \mathcal{S}_{sem,i} + \mathcal{S}_{temp,i} + w_{edge}E_i \quad (13)$$

Here,  $w_{edge}$  denotes the weight coefficient for the geometric prior. The term  $w_{edge}E_i$  ensures that physical contours, referred to as Structural Anchors, retain high weights even in regions with weak semantic or motion signals. Finally, we reconstruct the refined visual sequence  $\hat{X}_t$  from the original dense features via an index gathering operation:

$$\hat{X}_t = \{x_i \in X^{vis} \mid x_i \in \mathcal{K}_t \vee \text{Score}_i > \theta_{geo}\} \quad (14)$$

Where  $\theta_{geo}$  denotes the predefined threshold controlling the minimum edge strength. The resulting compact visual sequence is concatenated with the text instruction sequence and fed into the subsequent LLM, enabling efficient and robust multimodal action reasoning.

## 4 Experiment

### 4.1 Experiments Setup

We evaluate the efficacy of our proposed training-free method across both simulation and real-world scenarios. Specifically, within the simulation environment, we integrate VLA-IAP with established open-source VLA backbones, including OpenVLA-OFT [11], DreamVLA [25],  $\pi_0$  [2] and  $\pi_{0.5}$  [10], and benchmark performance on LIBERO [15], VLABench [24], and CALVIN [16]. To ensure a comprehensive evaluation, we further validate our approach on a custom-built robot platform in real-world settings. Experiments run on Linux with an NVIDIA A100.

**Table 1. Comprehensive Performance Comparison.** We evaluate **DreamVLA**,  $\pi_0$  (LIBERO) and  $\pi_{0.5}$  (VLABench) across multiple benchmarks under varying token retention ratios. **Ours (VLA-IAP)** demonstrates superior overall robustness and higher average success rates ( $\uparrow$ ), especially in complex reasoning tasks.

	LIBERO Success (%)				DreamVLA							OpenPi ( $\pi_0, \pi_{0.5}$ )						
	Spa.	Obj.	Goal	Long	CALVIN (Seq. Length $\uparrow$ )					Avg.	Spa.	Obj.	Goal	Long	VLABench Success (%)			
					1	2	3	4	5						Con.	Paint.	Poker.	Avg.
Vanilla	84.5	91.5	89.5	89.5	<i>Upper Bound (Vanilla / 100% Retention)</i>													
					97.8	94.5	89.5	83.8	77.5	4.43	94.2	98.2	94.6	82.8	56.0	30.0	52.0	46.0
					<i>Retain 70% Tokens (Pruning Ratio 30%)</i>													
FastV	86.5	86.5	84.0	87.5	97.6	94.5	89.0	82.8	76.8	4.40	93.5	96.1	92.2	80.5	44.0	28.0	32.0	34.6
SparseVLM	86.5	85.0	91.5	86.5	97.4	93.8	88.6	83.0	76.8	4.40	93.8	94.8	92.5	80.1	50.0	32.0	26.0	36.0
DivPrune	85.5	90.5	88.0	85.5	98.0	94.3	88.9	83.4	<b>78.3</b>	4.42	91.8	92.5	91.4	79.2	6.0	22.0	2.0	10.0
VLA-Cache	88.0	89.5	89.5	87.5	98.2	94.8	89.2	82.5	77.1	4.42	94.5	97.8	94.5	82.6	42.0	32.0	<b>48.0</b>	40.7
<b>Ours (VLA-IAP)</b>	<b>91.5<math>\uparrow</math></b>	<b>93.5<math>\uparrow</math></b>	<b>92.5<math>\uparrow</math></b>	<b>90.5<math>\uparrow</math></b>	<b>98.4<math>\uparrow</math></b>	<b>95.1<math>\uparrow</math></b>	<b>89.7</b>	<b>83.7<math>\uparrow</math></b>	<b>78.0<math>\uparrow</math></b>	<b>4.45<math>\uparrow</math></b>	<b>94.8<math>\uparrow</math></b>	<b>98.5<math>\uparrow</math></b>	<b>95.2<math>\uparrow</math></b>	<b>84.2<math>\uparrow</math></b>	<b>55.0</b>	<b>36.0<math>\uparrow</math></b>	<b>48.0</b>	<b>46.3<math>\uparrow</math></b>
					<i>Retain 50% Tokens (Pruning Ratio 50%)</i>													
FastV	84.5	81.5	84.0	86.5	94.2	92.8	84.5	79.7	70.1	4.21	92.4	95.3	91.0	79.4	16.0	22.0	2.0	13.3
SparseVLM	84.5	83.5	<b>90.5</b>	86.5	97.9	94.2	89.1	82.9	76.1	4.40	92.0	93.8	90.7	77.6	14.0	30.0	2.0	15.3
DivPrune	84.5	<b>92.0</b>	84.5	85	98.3	93.4	84.9	80.3	74.3	4.32	88.8	92.0	89.8	75.3	4.0	22.0	2.0	9.3
VLA-Cache	87.5	88.0	86.0	87.5	98.1	92.5	89.0	82.1	76.8	4.39	94.1	95.9	<b>94.8</b>	82.0	16.8	30.0	11.3	19.3
<b>Ours (VLA-IAP)</b>	<b>90.5<math>\uparrow</math></b>	<b>92.0<math>\uparrow</math></b>	<b>90.5<math>\uparrow</math></b>	<b>89.7<math>\uparrow</math></b>	<b>98.4<math>\uparrow</math></b>	<b>94.3</b>	<b>89.4</b>	<b>83.5</b>	<b>77.9<math>\uparrow</math></b>	<b>4.44<math>\uparrow</math></b>	<b>94.5<math>\uparrow</math></b>	<b>98.3<math>\uparrow</math></b>	94.5	<b>83.4<math>\uparrow</math></b>	<b>48.9</b>	<b>32.0<math>\uparrow</math></b>	<b>42.0</b>	<b>41.0</b>
					<i>Retain 30% Tokens (Pruning Ratio 70%)</i>													
FastV	79.0	56.5	73.0	81.5	89.8	85.2	78.2	71.5	63.5	3.88	86.8	80.7	86.2	73.9	0.0	22.0	0.0	7.3
SparseVLM	76.5	43.0	79.0	80.5	96.3	90.9	83.5	74.4	66.3	4.11	87.1	86.2	82.5	71.9	18.0	26.0	2.0	15.3
DivPrune	71.0	87.5	81.5	80.5	96.8	90.8	85.0	76.8	69.8	4.19	82.1	72.2	79.4	66.0	4.0	16.0	0.0	6.7
VLA-Cache	81.5	81.5	79.2	79.5	97.1	90.2	82.6	78.5	68.6	4.17	86.5	87.2	85.6	72.6	0.0	24.0	0.0	8.0
<b>Ours (VLA-IAP)</b>	<b>87.5<math>\uparrow</math></b>	<b>89.5</b>	<b>89.2</b>	<b>89.1</b>	<b>97.8<math>\uparrow</math></b>	<b>94.7<math>\uparrow</math></b>	<b>89.6<math>\uparrow</math></b>	<b>83.5</b>	<b>76.4</b>	<b>4.42</b>	<b>93.2</b>	<b>97.6</b>	<b>94.2</b>	<b>82.6</b>	<b>46.0</b>	<b>32.0<math>\uparrow</math></b>	<b>22.0</b>	<b>33.3</b>

## 4.2 Evaluation Benchmark

**Simulation Benchmark.** As shown in Fig. 3, the simulation evaluation spans three complementary benchmarks: LIBERO [15], CALVIN [16], and VLABench [24], designed to cover distinct capability dimensions. LIBERO focuses on generalization under lifelong learning settings, encompassing spatial, object, goal, and long-horizon task variations. CALVIN emphasizes long-horizon language-conditioned policy learning, testing task continuity and contextual memory. VLABench introduces more challenging complex long-horizon reasoning tasks. For VLABench, we report detailed results on three representative task subsets (add\_condiment, select\_painting, select\_poker) in the main paper, while full benchmark data is provided in the Supplementary Material.

**Real-World Experiments.** To evaluate the generalizability and real-time control capabilities of VLA-IAP, we deployed our framework on a physical robotic platform equipped with both global and wrist-mounted cameras. Evaluations were performed on both single-arm and dual-arm manipulators, as depicted in Fig. 4. Specifically, we designed three manipulation tasks of varying complexity to assess precision and robustness against environmental distractors: (1) *Simple*, involving picking a bowl and placing it into a plate; (2) *Long*, a multi-step sequence requiring placing a bowl into a plate followed by placing bread into the bowl; and (3) *Dual-arm*, coordinating two arms to sort hazardous and non-hazardous waste into respective bins. We benchmark VLA-IAP against the unpruned foundation baseline  $\pi_{0.5}$ . Additional implementation details and hyperparameters are provided in the Supplementary Material.

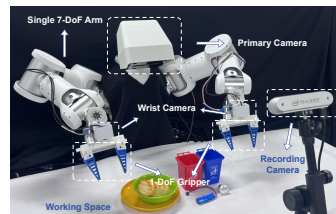


**Fig. 4.** Real Robot Experiment Setup

**Table 2. OpenVLA-OFT Results on LIBERO Benchmark.** Comparison of VLA models (Part I) and pruning methods (Part II) using OFT (7B) backbone.

Method	CKPT	Success Rate (%)					Speedup
		Spa.	Obj.	Goal	Long	Avg.	
<i>Part I: Vision-Language-Action Models</i>							
OpenVLA [12]	OpenVLA (7B)	84.7	88.4	79.2	53.7	76.5	-
WorldVLA [4]	Cham. (7B)	87.6	96.2	83.4	60.0	81.8	-
NORA [9]	Qwen-VL (3B)	85.6	87.8	77.0	45.0	73.9	-
SmolVLA [18]	SmolVLM (2.2B)	93.0	94.0	91.0	77.0	88.8	-
CogACT [13]	CogVLM (7B)	97.2	98.0	90.2	88.8	93.6	-
OpenVLA-OFT [11]	OFT (7B)	98.6	98.2	96.6	94.8	97.1	1.00×
<i>Part II: Pruning Methods</i>							
VLA-ADP [17] (Ratio=70%)	OFT (7B)	99.0	98.2	96.8	91.2	96.3	1.13×
VLA-ADP [17] (Ratio=50%)	OFT (7B)	<b>99.4</b>	98.0	96.4	91.2	96.3	1.23×
VLA-ADP [17] (Ratio=30%)	OFT (7B)	97.6	98.4	97.4	84.2	94.4	1.35×
FastV [5]	OFT (7B)	96.8	81.0	96.4	73.0	86.8	1.24×
VLA-Cache [21]	OFT (7B)	98.3	97.5	98.3	95.4	97.4	1.30×
SpecPrune-VLA [19]	OFT (7B)	98.2	96.3	97.7	94.0	96.6	1.46×
TeamVLA [23]	OFT (7B)	99.2	96.5	97.0	93.8	96.6	1.51×
EfficientVLA [22]	OFT (7B)	96.5	91.1	96.0	72.1	88.9	<b>1.54×</b>
<b>VLA-IAP (Ratio=70%)</b>	OFT (7B)	97.6	<b>99.6</b>	<b>98.4</b>	<b>95.6</b>	<b>97.8</b>	1.25×
<b>VLA-IAP (Ratio=50%)</b>	OFT (7B)	97.3	99.1	98.2	95.2	97.5	1.37×
<b>VLA-IAP (Ratio=30%)</b>	OFT (7B)	96.6	98.8	98.0	94.8	97.1	<b>1.54×</b>

### 4.3 Results on Simulation Environments

**Comprehensive Performance Comparison.** Tab. 1 compares VLA-IAP against baselines across varying token retention rates. Evaluation spans three VLA backbones and three benchmarks focusing on generalization, long-horizon actions, and complex reasoning. While all methods degrade with lower retention, VLA-IAP demonstrates superior robustness. At 70% retention, VLA-IAP surpasses the unpruned baseline on multiple metrics, achieving a 4.45 average sequence length on CALVIN and 46.3% success rate on VLABench. This indicates our dynamic alignment strategy accelerates inference while filtering visual noise to enhance policy focus.

Performance divergence becomes critical at 30% retention on the challenging VLABench. VLABench tasks require precise geometric perception and fine manipulation control. Under extreme compression, FastV and SparseVLM suffer catastrophic failures, with DivPrune dropping to only 6.7% success. This exposes a fundamental flaw in perception-first methods inherited from traditional VLMs. Although VLA-Cache accounts for the temporal continuity in robotic tasks by caching historical features, it only maintains a relatively higher accuracy (40.7%) when retaining 70% of the tokens. Once the retention drops to 30%, its performance collapses rapidly to 8.0%. As revealed in Section 1, their reliance on static semantic saliency or global feature diversity results in discrete and fragmented visual representations. Such pruning logic destroys local geometric continuity essential for manipulation, leaving the model without spatial physical references. In contrast, VLA-IAP maintains a 33.3% success rate under these extreme conditions. These results validate our Interaction-First paradigm and geometric prior mechanism detailed in Section 3. VLA-IAP actively preserves structural anchors required for physical operations. This prevents target sparsification caused by prioritizing semantic diversity, ensuring action coherence and precision even under extreme compression.

**OpenVLA-OFT Results on LIBERO.** Tab. 2 presents the performance of various Vision-Language-Action models and pruning methods on the LIBERO benchmark. The unpruned OpenVLA-OFT backbone establishes a strong baseline with a 97.1% average success rate. VLA-IAP achieves a state-of-the-art average success rate of 97.8% and a 1.25 $\times$  inference speedup at a 70% token retention ratio. This performance effectively surpasses the unpruned baseline to demonstrate the benefit of our geometric and dynamic pruning mechanisms. Existing acceleration methods typically sacrifice significant manipulation capabilities to gain efficiency. EfficientVLA delivers a 1.54 $\times$  speedup but suffers a severe performance drop to an 88.9% average success rate. Our method conversely maintains a 97.1% average success rate under the aggressive 30% token retention setting. This configuration yields a 1.54 $\times$  speedup to perfectly match the original model accuracy. These results demonstrate that VLA-IAP establishes an optimal balance between execution accuracy and inference efficiency across different compression targets.

**Ablation Study.** Tab. 3 presents a component-wise ablation study to validate the progressive integration of VLA-IAP into the unpruned OpenVLA-OFT baseline, which initially yields a 94.5% success rate and a 123.2 ms latency. We first replace static attention with a base spatiotemporal module that independently calculates and fuses semantic and temporal scores to retain the top-K tokens. This modification effectively filters background noise, reducing the latency to 86.7 ms for a 1.42 $\times$  speedup while achieving a 94.8% success rate. We then upgrade this rigid top-K selection to an IoU-guided dynamic strategy with a threshold of 0.05 to prevent the premature loss of crucial manipulation targets during highly uncertain early phases. Monitoring the semantic-motion alignment to adaptively toggle pruning intensity increases the success rate to 97.2% with a 93.3 ms latency. Finally, incorporating edge enhancement with a weight of 1.0 establishes our optimal configuration. This setup achieves a 97.8% success rate and maintains a 1.25 $\times$  speedup with a 98.6 ms latency. This consistent performance improvement validates our Interaction-First hypothesis. Explicitly preserving geometrically sharp contours as structural anchors corrects the semantic bias inherited from standard VLM pruning and ensures the physical continuity essential for precise robotic manipulation.

**Runtime Analysis.** Tab. 4 details the hardware efficiency of the evaluated acceleration methods by measuring peak GPU memory usage and CUDA runtime per step. The unpruned baseline consumes 7.11 GB of memory with a latency

**Table 3. Component-wise Ablation.** Progressive integration of Spatiotemporal Pruning, IoU-Guided Switching, and Edge Enhancement.

Method	SR (%)	Latency (ms)	Speedup
OpenVLA-OFT (Base)	94.5	123.2	1.00 $\times$
<i>Step 1: Spatiotemporal Pruning (<math>k \ \ell \ \gamma</math>)</i>			
+ Spatiotemp. ( $k = 0.3, \gamma = 0.7$ )	93.1	77.9	1.58 $\times$
<b>+ Spatiotemp. (<math>k = 0.5, \gamma = 0.7</math>)</b>	<b>94.8</b>	<b>86.7</b>	<b>1.42<math>\times</math></b>
+ Spatiotemp. ( $k = 0.7, \gamma = 0.7$ )	92.5	94.8	1.30 $\times$
<i>Step 2: IoU-Guided Switching</i>			
+ IoU Threshold ( $\theta_{iou} = 0.02$ )	95.1	78.9	1.56 $\times$
<b>+ IoU Threshold (<math>\theta_{iou} = 0.05</math>)</b>	<b>97.2</b>	<b>93.3</b>	<b>1.32<math>\times</math></b>
+ IoU Threshold ( $\theta_{iou} = 0.10$ )	95.5	97.0	1.27 $\times$
<i>Step 3: Edge Enhancement (Final)</i>			
<b>+ Edge Weight (<math>\theta_{iou} = 0.05, w_{edge} = 1.0</math>)</b>	<b>97.8</b>	<b>98.6</b>	<b>1.25<math>\times</math></b>
+ Edge Weight ( $\theta_{iou} = 0.05, w_{edge} = 0.5$ )	97.2	97.0	1.27 $\times$
+ Edge Weight ( $\theta_{iou} = 0.05, w_{edge} = 1.5$ )	97.4	96.3	1.28 $\times$
<b>+ Edge Weight (<math>\theta_{iou} = 0.02, w_{edge} = 1.0</math>)</b>	<b>97.1</b>	<b>80.0</b>	<b>1.54<math>\times</math></b>

**Table 4. Memory and Runtime Analysis of Acceleration Methods on  $\pi_0$**  across VLABench. Detailed comparison of maximum GPU memory consumption and CUDA runtime across different vision-token retention rates.

Method	70% Retained		50% Retained		30% Retained	
	Max Memory (GB) ↓	CUDA Time (ms) ↓	Max Memory (GB) ↓	CUDA Time (ms) ↓	Max Memory (GB) ↓	CUDA Time (ms) ↓
Vanilla	Origin Memory: 7.11 GB / Origin CUDA Latency: 98.03 ms					
FastV	7.018	81.69	6.989	74.27	6.968	69.52
SparseVLM	7.003	81.02	6.961	72.61	6.954	70.53
DivPrune	6.961	79.69	<b>6.925</b>	73.16	6.911	69.04
VLA-Cache	7.082	88.32	7.067	83.79	7.032	79.69
VLA-IAP(Ours)	<b>6.998</b>	<b>77.96</b>	6.932	<b>72.08</b>	<b>6.882</b>	<b>65.79</b>

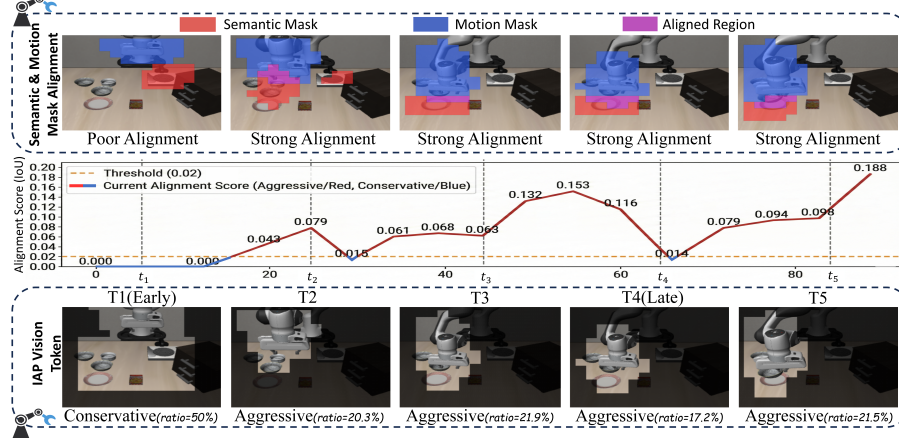


**Fig. 5. Visualization of Interaction-aligned Pruning Process on LIBERO.** (Bottom) Dynamic shift in visual token retention from conservative to aggressive mode. (Middle) The alignment score (IoU) regulating the pruning state. (Top) The overlap (purple) between semantic intent (red) and arm motion (blue) masks that drives the alignment score.

of 98.03 ms. At a 50% retention rate, VLA-IAP reduces the memory footprint to 6.932 GB and the runtime to 72.08 ms. This reduction establishes a highly competitive resource consumption profile among all tested methods. The efficiency advantage remains consistent across more aggressive pruning settings. At a 30% retention rate, our method achieves an inference latency of 65.79 ms and a memory footprint of 6.882 GB. These performance improvements ensure stable deployment on physical robotic platforms.

**Visualization on Simulation Experiment.** Fig. 5 visualizes the internal mechanism of the spatiotemporal alignment pruning process during a complete manipulation episode on the LIBERO dataset. The bottom row demonstrates poor alignment during the initial approach phase at time  $t_1$  where the semantic mask and the motion mask share no overlapping regions. The middle plot consequently displays an Intersection over Union alignment score of zero which strictly falls below the fixed threshold. This low confidence state triggers the conservative mode shown in the top row. The model retains most objects and only prunes background pixels to prevent the premature loss of the manipulation target. The semantic and motion masks intersect to form a purple overlapping region as the robot arm approaches the target at time  $t_2$  and beyond. The align-

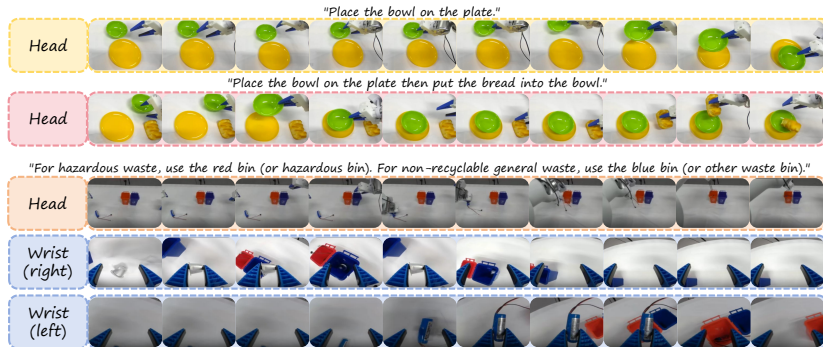


**Fig. 6. Real-World Task Demonstrations.** From top to bottom: simple (single-step), long-horizon (multi-step), and dual-arm (coordinated) manipulation tasks, showing head and wrist camera perspectives.

ment score explicitly rises above the threshold to indicate strong alignment and high confidence. This state activates the aggressive pruning mode where the model filters out irrelevant objects to heavily compress the visual tokens. This adaptive mechanism ensures optimal pruning efficiency under high confidence states while effectively preventing mistaken pruning during early exploration.

#### 4.4 Results on Real Robot

Tab. 5 shows that VLA-IAP achieves  $1.48\times$  and  $1.47\times$  latency reduction on single-arm and dual-arm tasks, respectively. Our method improves success rates on simple (+4.0%) and long-horizon (+4.0%) tasks while matching the baseline on dual-arm coordination (44.0%). Overall, VLA-IAP increases the average success rate to 65.3% while significantly reducing inference latency. Fig. 6 visualizes successful execution examples across these three task categories, confirming robust performance under different camera perspectives.

## 5 Conclusion

In this paper, we propose VLA-IAP, a training-free visual token pruning framework that shifts embodied visual compression from a passive Perception-First bias to an explicit Interaction-First paradigm. Our empirical results reveal that relying solely on semantic saliency leads to catastrophic failures in precise robotic manipulation, highlighting the critical need to preserve geometric continuity. By integrating edge-enhanced structural anchors with an adaptive semantic-motion

**Table 5. Real-World Experiments (3 tasks).** Task 1–3 cover simple, long, and dual-arm challenge tasks.

Success Rate (%)				
Method	Simple	Long	Dual-Arm	Avg.
$\pi_{0.5}$ (base)	80.0	64.0	44.0	62.7
<b>VLA-IAP</b>	<b>84.0</b>	<b>68.0</b>	44.0	<b>65.3</b>
Latency (ms) ↓				
Method	Single	Dual		
$\pi_{0.5}$ (base)	88.1	124.3		
<b>VLA-IAP</b>	<b>59.7 (1.48×)</b>	<b>84.6 (1.47×)</b>		

alignment strategy, VLA-IAP successfully filters redundant background noise while safeguarding critical physical affordances. Extensive evaluations across challenging simulation benchmarks and real-world deployments confirm that our method achieves state-of-the-art inference acceleration without compromising task robustness.

# Supplementary Material

## A Method Details

**Algorithm Outlines.** We detail the mathematical formulation of the multi-dimensional physical priors in **Algorithm 1**, and the overall interaction-aligned dynamic token selection strategy in **Algorithm 2**.

---

### Algorithm 1 Multi-Dimensional Physical Priors Construction

---

**Require:** Current and historical observations  $I_t, I_{t-1}, I_{t-2}$ , language instruction  $Inst$ , temperature  $\tau$ , decay factor  $\gamma$

**Ensure:** Geometric prior  $E$ , Semantic prior  $\mathcal{S}_{\text{sem}}$ , Motion prior  $\mathcal{S}_{\text{temp}}$ , visual embeddings  $X^{\text{vis}}$

- 1: **1. Feature Initialization:**
  - 2:  $X^{\text{vis}} \leftarrow \text{VisionEncoder}(I_t)$ ,  $\hat{e}_{\text{text}} \leftarrow \text{TextEncoder}(Inst)$   $\triangleright N \times D$  visual tokens
  - 3: **2. Geometric Prior (Edge Enhancement):**
  - 4:  $I_{\text{gray}} \leftarrow \text{Grayscale}(I_t)$
  - 5: Compute directional gradients:  $G_x \leftarrow I_{\text{gray}} * K_x$ ,  $G_y \leftarrow I_{\text{gray}} * K_y$   $\triangleright$  Eq. 1
  - 6: Pixel-level edge magnitude:  $\mathcal{G}(u, v) \leftarrow \sqrt{G_x(u, v)^2 + G_y(u, v)^2}$   $\triangleright$  Eq. 2
  - 7: Aggregate to patch-level  $E_i \leftarrow \frac{1}{|\mathcal{P}_i|} \sum_{(u, v) \in \mathcal{P}_i} \mathcal{G}(u, v)$  for  $i \in \{1, \dots, N\}$   $\triangleright$  Eq. 3
  - 8: Normalize  $E \leftarrow \text{MinMax}(E)$
  - 9: **3. Semantic Prior:**
  - 10: Cross-modal alignment  $p_i \leftarrow \frac{\exp((X_i^{\text{vis}} \cdot \hat{e}_{\text{text}}) / \tau)}{\sum_j \exp((X_j^{\text{vis}} \cdot \hat{e}_{\text{text}}) / \tau)}$   $\triangleright$  Eq. 4
  - 11:  $\mathcal{S}_{\text{sem}} \leftarrow \text{MinMax}(\text{AvgPool}(p))$
  - 12: **4. Motion Prior (Temporal Kinematics):**
  - 13: 2nd-order diff:  $d_{t,i} \leftarrow \|X_{t,i}^{\text{vis}} - 2X_{t-1,i}^{\text{vis}} + X_{t-2,i}^{\text{vis}}\|_2$   $\triangleright$  Eq. 5
  - 14: Reshape  $d_t$  to 2D grid  $M_t$
  - 15: History Accumulation:  $H_t \leftarrow (1 - \gamma)M_t + \gamma H_{t-1}$   $\triangleright$  Eq. 6
  - 16: Morphological & Gaussian smoothing:  $\tilde{M}_t \leftarrow ((H_t \oplus K_{\text{str}}) \ominus K_{\text{str}}) * \mathcal{N}(0, \sigma^2)$   $\triangleright$  Eq. 7
  - 17: Flatten  $\tilde{M}_t$  to 1D and Normalize  $\mathcal{S}_{\text{temp}} \leftarrow \text{MinMax}(\tilde{M}_t)$
  - 18: **return**  $E, \mathcal{S}_{\text{sem}}, \mathcal{S}_{\text{temp}}, X^{\text{vis}}$
- 

## B Experiments Details

### B.1 VLA Models Details

In our evaluations, we benchmark VLA-IAP against several state-of-the-art Vision-Language-Action (VLA) foundation models to demonstrate its broad applicability.

---

**Algorithm 2** Interaction-Aligned Dynamic Token Selection

---

**Require:** Priors  $\{E, \mathcal{S}_{\text{sem}}, \mathcal{S}_{\text{temp}}\}$ , visual embeddings  $X^{\text{vis}}$ , thresholds  $\{\theta_{\text{iou}}, \theta_{\text{geo}}, w_{\text{edge}}, k, k_{\text{bg}}, r\}$

**Ensure:** Selected compact visual tokens  $\hat{X}_t$

- 1: **1. Semantic-Motion Alignment Scoring:**
- 2: Binarize intent mask:  $\mathcal{B}_{\text{sem}} \leftarrow \mathbb{I}(\mathcal{S}_{\text{sem}} > \mu_{\text{sem}} + k \cdot \sigma_{\text{sem}})$  ▷ Eq. 8
- 3: Binarize motion mask:  $\mathcal{B}_{\text{temp}} \leftarrow \mathbb{I}(\mathcal{S}_{\text{temp}} > \mu_{\text{temp}} + k \cdot \sigma_{\text{temp}})$
- 4: Compute gating metric:  $\text{IoU}_t \leftarrow \frac{|\mathcal{B}_{\text{sem}} \cap \mathcal{B}_{\text{temp}}|}{|\mathcal{B}_{\text{sem}} \cup \mathcal{B}_{\text{temp}}|}$  ▷ Eq. 9
- 5: **2. Adaptive Mode Switching:**
- 6: **if**  $\text{IoU}_t \leq \theta_{\text{iou}}$  **then** ▷ Conservative Mode (Exploration)
- 7:   Joint background  $\mathcal{B}_{\text{bg}} \leftarrow \mathbb{I}(\mathcal{S}_{\text{sem}} < \mu_{\text{sem}} + k_{\text{bg}} \sigma_{\text{sem}}) \wedge \mathbb{I}(\mathcal{S}_{\text{temp}} < \mu_{\text{temp}} + k_{\text{bg}} \sigma_{\text{temp}})$   
  ▷ Eq. 10
- 8:   Base retention set  $\mathcal{K}_t \leftarrow \{x_i \in X^{\text{vis}} \mid \mathcal{B}_{\text{bg},i} = 0\}$  ▷ Double-weak exclusion
- 9: **else** ▷ Aggressive Mode (Interaction Lock)
- 10:   Locate semantic center  $c^* \leftarrow \arg \max_i \mathcal{S}_{\text{sem},i}$
- 11:   Contract to core region  $\mathcal{B}_{\text{sem}}^{\text{core}} \leftarrow \mathcal{B}_{\text{sem}} \wedge \mathbb{I}(\text{dist}(x_i, c^*) \leq r)$
- 12:   Base retention set  $\mathcal{K}_t \leftarrow \{x_i \in X^{\text{vis}} \mid (\mathcal{B}_{\text{sem},i}^{\text{core}} \vee \mathcal{B}_{\text{temp},i}) = 1\}$  ▷ Eq. 11
- 13: **end if**
- 14: **3. Final Affordance-Guided Gathering:**
- 15: **for each** token index  $i \in \{1, \dots, N\}$  **do**
- 16:   Compute comprehensive priority  $\text{Score}_i \leftarrow \mathcal{S}_{\text{sem},i} + \mathcal{S}_{\text{temp},i} + w_{\text{edge}} E_i$  ▷ Eq. 13
- 17: **end for**
- 18: Reconstruct sequence  $\hat{X}_t \leftarrow \{x_i \in X^{\text{vis}} \mid x_i \in \mathcal{K}_t \vee \text{Score}_i > \theta_{\text{geo}}\}$  ▷ Eq. 14
- 19: **return**  $\hat{X}_t$

---

**OpenVLA-OFT.** OpenVLA-OFT [11] builds upon the open-source OpenVLA architecture, which fuses a dual vision backbone (SigLIP + DINOv2) with a Llama-2 7B language model via a 3-layer MLP projector. The OFT (Optimized Fine-Tuning, not Orthogonal Finetuning) variant integrates three core optimizations: parallel decoding with action chunking (to enhance inference efficiency and temporal consistency), continuous action representations (replacing discrete tokenization for higher precision), and an L1 regression objective (for faster convergence and inference). For bimanual tasks requiring strong language grounding, the augmented OFT+ variant further incorporates FiLM (feature-wise linear modulation) to suppress spurious visual correlations. In our experiments, we utilize the 7B parameter version and follow the default multimodal prompt formatting for instruction conditioning, including support for multi-view images (third-person + wrist-mounted) and robot proprioceptive state inputs.

**OpenPi ( $\pi_0$  and  $\pi_{0.5}$ ).** Developed by Physical Intelligence [2,10],  $\pi_0$  and its enhanced version  $\pi_{0.5}$  are vision-language-action (VLA) models built on a PaliGemma VLM backbone. They adopt conditional flow matching (a variant of diffusion) for continuous action generation, enabling high-frequency (up to 50 Hz) dexterous control and cross-embodiment generalization. A key design is the "action expert"—a separate set of weights specialized for flow-based action chunk prediction—paired with a pre-training/post-training recipe (diverse cross-robot

data + task-specific fine-tuning).  $\pi_{0.5}$  extends this framework with co-training on heterogeneous data (web multimodal data, high-level subtask prediction, verbal instructions) to enable open-world generalization in unseen environments. For inference, we maintain the default 10 integration steps (flow matching) and feed visual tokens, language instructions, and robot proprioceptive state into their cross-attention conditioning modules.

**DreamVLA.** DreamVLA [25] is a perception-prediction-action framework that integrates comprehensive world knowledge forecasting (dynamic regions, depth maps, DINOv2/SAM semantic features) to facilitate inverse dynamics modeling. It adopts a unified transformer architecture with: a MAE-pretrained ViT visual encoder, CLIP text encoder, MLP-based robot state encoder, learnable  $\text{jdream}$  queries (for world knowledge prediction), and a diffusion-transformer decoder (DiT-B) for action generation. A block-wise structured attention mechanism prevents cross-type knowledge leakage between dynamic/spatial/semantic features. In our experiments, we evaluate DreamVLA using its standard pre-trained checkpoint, applying our pruning masks to its vision encoder outputs (after Perceiver Resampler condensation) before processing by the GPT-2 Medium backbone.

## B.2 Compression Methods Details

To validate the superiority of our Interaction-First paradigm, we compare VLA-IAP against four representative visual token compression baselines. All methods are evaluated under identical target retention ratios (70%, 50%, and 30%) for fair comparison.

**FastV.** FastV [5] is a training-free, plug-and-play pruning method designed for Large Vision-Language Models (LVLMs). It addresses intra-frame redundancy by leveraging the inefficient visual attention phenomenon in LVLMs: image tokens receive drastically lower attention scores than text tokens after the first 2 layers. FastV dynamically prunes visual tokens at a predefined layer  $K$  (default  $K=2$ ) by ranking tokens based on their average received attention scores—tokens below a threshold are discarded in subsequent layers. This strategy eliminates redundant computations in both self-attention and feed-forward network (FFN) modules, without requiring model retraining.

**SparseVLM.** SparseVLM [26] is a text-guided, training-free token sparsification method for VLMs. It first selects relevant text tokens (raters) via cross-attention (filtering out irrelevant text like prepositions), then uses these raters to evaluate the significance of visual tokens based on self-attention matrices. Instead of direct truncation, it employs a rank-based adaptive sparsification ratio (per layer) and a token recycling mechanism: pruned tokens are clustered (via density peak aggregation) and reconstructed into compact representations to minimize information loss. It optimizes computation by retaining high-significance visual tokens while compressing redundant ones.

**DivPrune.** DivPrune [1] is a diversity-centric token pruning strategy formulated as a Max-Min Diversity Problem (MMDP). It measures feature-level similarity (cosine distance) among all visual tokens in a frame, aiming to select a subset that maximizes the minimum pairwise distance between tokens. This ensures the retained tokens have high global diversity and low redundancy, without relying on attention scores or text guidance.

**VLA-Cache.** VLA-Cache [21] is a training-free inference acceleration method tailored for Vision-Language-Action (VLA) models in robotic manipulation. It targets temporal redundancy across consecutive frames: first identifying static visual tokens via patch similarity, then filtering out task-relevant tokens (via decoder cross-attention scores) to avoid reusing semantically critical regions. A layer-adaptive strategy dynamically adjusts the token reuse ratio based on attention entropy.

### B.3 Benchmark Details

Our comprehensive evaluation spans three simulation environments and a real-world robotic setup, designed to test distinct axes of embodied intelligence.

**LIBERO.** LIBERO [15] is a benchmark dedicated to lifelong learning in robotic manipulation, focusing on the transfer of both declarative (e.g., object concepts, spatial relationships) and procedural (e.g., actions, behaviors) knowledge. It consists of four procedurally generated task suites with distinct distribution shifts: *LIBERO-Spatial* (fixed objects and layouts, varying spatial relationships between entities), *LIBERO-Object* (fixed layouts, novel object categories requiring new concept learning), *LIBERO-Goal* (fixed objects and spatial layouts, distinct task goals demanding new motor skills), and *LIBERO-100* (100 diverse tasks with entangled knowledge transfer, including 90 short-horizon tasks and 10 long-horizon *LIBERO-Long* tasks). All tasks are inspired by everyday human activities, sharing visual concepts and interaction patterns to facilitate systematic study of knowledge transfer and anti-forgetting in lifelong learning.

**VLABench.** VLABench [24] is a large-scale language-conditioned robotic manipulation benchmark featuring 100 task categories, including 60 primitive tasks and 40 composite tasks. Primitive tasks are categorized into five core ability dimensions: mesh and texture understanding (recognizing complex object shapes and textures), spatial understanding (interpreting relative positional relationships), common sense and world knowledge (transferring pre-trained knowledge to task execution), semantic understanding (extracting implicit goals from natural language instructions), and physical law adherence (applying physical principles to interactions). Composite tasks integrate multiple skills, requiring long-horizon planning (average episode length  $\geq 500$  timesteps) and multi-step logical reasoning, such as game rule application, multi-step ingredient preparation, and

device operation sequences. The benchmark includes over 2000 3D objects across 163 categories, with strong domain randomization (object positions, textures, lighting) to evaluate generalization.

**CALVIN.** CALVIN [16] focuses on long-horizon language-conditioned continuous control, comprising 34 manipulation tasks across four structurally related indoor environments (A/B/C/D). Environments share core elements (7-DOF Franka robot, desk, drawer, sliding door, colored blocks, light switch/button) but differ in textures and the spatial positions of static components. The 34 tasks cover block manipulation (rotation, pushing, lifting, stacking), drawer/sliding door operation, and light control, which can be combined into long-horizon sequences of up to 5 consecutive sub-tasks. A key feature is zero-shot generalization evaluation: training on three environments and testing on the fourth unseen environment, with unconstrained natural language instructions to specify tasks (e.g., "open the drawer and push the blue block inside").

#### B.4 Real Robot.

**Robot Platform.** Our real-world evaluations are conducted on a self-developed dual-arm robotic system. The platform consists of two symmetric **7-DoF robotic arms**, providing a total of 14 degrees of freedom (DoF), each integrated with a **1-DoF parallel-jaw gripper**. The entire system is mounted on a fixed base to maintain a stable workspace for coordinated manipulation tasks.

**Sensing and Perception.** The visual observation space is captured by a multi-camera setup:

- **Global View:** A **ZED 2i binocular camera** is fixed to the robot’s head. Only the RGB stream from the **left lens** is used for VLA model training and inference.
- **Wrist View:** Each arm is equipped with a wide-angle RGB wrist-mounted camera. Single-arm tasks utilize the head camera and the active arm’s wrist camera, while dual-arm tasks utilize all three cameras (head and both wrists).
- **Data Specifications:** All observations are standardized to a resolution of **640×480**. An auxiliary **Intel RealSense D455** is used solely for external experimental recording and does not participate in the VLA inference pipeline.

**Runtime and Inference.** All policies are deployed on a Linux workstation running **Ubuntu 22.04** with a single **NVIDIA A100 GPU**. Our **VLA-IAP** framework is implemented on the  $\pi_{0.5}$  backbone. We utilize a training **chunk size of 50**, while during inference, only the **first 20 actions** of each predicted chunk are executed to ensure high-fidelity control.

**Table 6. Comprehensive Hardware Efficiency Analysis on Remaining Benchmarks.** We report the Maximum GPU Memory (GB) and CUDA Runtime (ms) for DreamVLA and  $\pi_0$  across different task suites and pruning ratios.

Method	70% Retained		50% Retained		30% Retained	
	Mem (GB) ↓	Time (ms) ↓	Mem (GB) ↓	Time (ms) ↓	Mem (GB) ↓	Time (ms) ↓
<b>DreamVLA (Benchmark: CALVIN)</b>						
Vanilla (100%)	Origin Memory: 2.810 GB / Origin CUDA Latency: 120.28 ms					
FastV	2.771	99.40	2.762	91.45	2.751	85.30
SparseVLM	2.764	99.41	2.758	89.09	2.746	86.53
DivPrune	2.756	<b>97.79</b>	2.748	89.76	2.731	84.72
VLA-Cache	2.798	102.43	2.790	97.78	2.779	93.22
<b>VLA-IAP (Ours)</b>	<b>2.747</b>	98.21	<b>2.732</b>	<b>88.54</b>	<b>2.719</b>	<b>82.95</b>
<b>DreamVLA (Benchmark: LIBERO)</b>						
Vanilla (100%)	Origin Memory: 2.661 GB / Origin CUDA Latency: 101.47 ms					
FastV	2.626	84.55	2.615	76.87	2.608	72.96
SparseVLM	2.621	83.85	2.612	75.16	2.602	73.76
DivPrune	2.615	82.49	2.594	75.72	2.586	72.45
VLA-Cache	2.634	85.99	2.628	84.56	2.621	80.14
<b>VLA-IAP (Ours)</b>	<b>2.610</b>	<b>81.89</b>	<b>2.582</b>	<b>74.61</b>	<b>2.574</b>	<b>69.97</b>
<b><math>\pi_0</math> (Benchmark: LIBERO)</b>						
Vanilla (100%)	Origin Memory: 6.214 GB / Origin CUDA Latency: 94.13 ms					
FastV	6.135	79.44	6.092	71.31	6.079	66.76
SparseVLM	6.117	79.80	6.082	70.83	6.074	67.72
DivPrune	6.109	76.53	6.076	71.85	6.052	67.24
VLA-Cache	6.185	84.85	6.147	80.45	6.141	76.53
<b>VLA-IAP (Ours)</b>	<b>6.098</b>	<b>75.44</b>	<b>6.069</b>	<b>69.73</b>	<b>6.032</b>	<b>64.82</b>

## B.5 More Results

**Efficiency across Diverse Architectures.** We provide a detailed hardware efficiency analysis in Table 6, evaluating peak GPU memory consumption and CUDA runtime across different VLA backbones and task suites. For DreamVLA, VLA-IAP consistently reduces memory overhead and inference latency across both CALVIN and LIBERO benchmarks, achieving significantly lower per-step runtimes compared to perception-first baselines like FastV and SparseVLM. Similar efficiency gains are observed on  $\pi_0$  backbone, where our method achieves the lowest latency of 64.82 ms at a 30% retention rate. These results confirm that VLA-IAP’s interaction-aligned strategy provides stable and hardware-friendly acceleration across varying model architectures and manipulation tasks, maintaining a competitive resource footprint essential for real-world deployment.

**The Full Benchmark Data of VLABench.** This section expands on the VLABench discussion in Section 4.3 of the main text to validate the robustness of the interaction-first paradigm against perception misalignment. As detailed in Table 7, under an extreme 30% token retention rate, perception-first baselines such as FastV and SparseVLM suffer catastrophic failures, dropping to a 0% success rate on multiple tasks including `select_flower` and `select_toy`. This collapse occurs because these methods rely entirely on the internal attention maps of the backbone network. As visualized in Fig. 9, the  $\pi_{0.5}$  model frequently misallocates attention to irrelevant backgrounds on these complex tasks, causing perception-first methods to discard critical manipulation targets.

**Table 7. Detailed Performance on VLABench Task Subsets.** Success rates (%) across 10 complex manipulation tasks under varying token retention ratios. Task names are abbreviated for brevity (e.g., ‘Con.’ for ‘add\_condiment’, ‘Chem.’ for ‘select\_chemistry\_tube’). **Ours (VLA-IAP)** consistently outperforms other baselines, maintaining robust manipulation capabilities even under extreme visual compression.

Method	Con.	Flower	Book	Chem.	Drink	Fruit	Mahj.	Paint.	Poker	Toy	Avg.
<i>Upper Bound (Vanilla / 100% Retention)</i>											
Baseline	56.0	20.0	54.0	36.0	42.0	42.0	32.0	30.0	52.0	28.0	39.2
<i>Retain 70% Tokens (↓ 30.0%)</i>											
FastV	44.0	2.0	38.8	35.4	18.0	2.0	2.1	28.0	32.0	2.0	20.4
SparseVLM	50.0	0.0	<b>52.2</b>	28.6	28.6	4.0	8.1	32.0	26.0	4.0	23.4
DivPrune	6.0	0.0	8.0	6.0	12.2	2.0	2.0	22.0	2.0	2.0	6.2
VLA-Cache	42.0	10.0	42.9	30.0	32.0	<b>30.0</b>	24.4	32.0	<b>48.0</b>	6.0	29.7
<b>VLA-IAP (Ours)</b>	<b>55.0</b>	<b>12.0</b>	40.4	<b>41.7</b>	<b>42.0</b>	26.0	<b>26.1</b>	<b>36.0</b>	<b>48.0</b>	<b>10.0</b>	<b>33.7</b>
<i>Retain 50% Tokens (↓ 50.0%)</i>											
FastV	16.0	0.0	25.6	8.2	18.4	0.0	2.1	22.0	2.0	0.0	9.4
SparseVLM	12.0	0.0	25.6	4.1	20.0	0.0	4.3	30.0	2.0	0.0	9.8
DivPrune	4.0	0.0	22.0	10.0	16.3	0.0	4.3	22.0	2.0	0.0	8.1
VLA-Cache	16.8	0.0	23.9	14.0	12.0	0.0	8.2	30.0	11.3	0.0	11.6
<b>VLA-IAP (Ours)</b>	<b>48.9</b>	<b>6.0</b>	<b>29.8</b>	<b>27.1</b>	<b>28.6</b>	<b>14.0</b>	<b>10.6</b>	<b>32.0</b>	<b>42.0</b>	<b>6.0</b>	<b>24.5</b>
<i>Retain 30% Tokens (↓ 70.0%)</i>											
FastV	0.0	0.0	21.5	0.0	4.3	0.0	2.1	22.0	0.0	0.0	5.0
SparseVLM	18.0	0.0	6.5	0.0	12.2	0.0	0.0	26.0	2.0	0.0	6.5
DivPrune	4.0	0.0	10.6	0.0	4.2	0.0	4.1	16.0	0.0	0.0	3.9
VLA-Cache	16.8	0.0	4.0	0.0	10.0	0.0	0.0	24.0	0.0	0.0	5.5
<b>VLA-IAP (Ours)</b>	<b>46.0</b>	<b>4.0</b>	<b>21.7</b>	<b>8.2</b>	<b>16.3</b>	<b>8.2</b>	<b>8.5</b>	<b>32.0</b>	<b>22.0</b>	<b>4.0</b>	<b>17.1</b>

VLA-IAP overcomes this limitation by utilizing edge-enhanced geometric priors and semantic-motion alignment, making the pruning process independent of the grounding quality of the language model. Consequently, VLA-IAP successfully avoids zero-success failures on the aforementioned difficult tasks and establishes a substantial performance gap on precision-demanding tasks, achieving 46.0% on add\_condiment and 22.0% on select\_poker. This mechanism enables VLA-IAP to sustain a 17.1% average success rate under extreme compression, empirically validating its structural advantage in preserving essential physical anchors.

**The Ablation of Different Edge Enhancement Methods.** To justify the selection of the Sobel operator, we conduct an ablation study comparing it against the traditional Canny[6] detector and two deep-learning-based edge extraction models, HED[20] and BDCN[7]. As summarized in Table 8, while deep-learning methods such as BDCN provide high-quality edge maps, they introduce significant computational overhead, increasing the per-step latency to 132.8 ms—surpassing even the unpruned baseline. Conversely, the Canny detector, although efficient, suffers from a performance drop (96.8% avg. success) due to its sensitivity to illumination changes and noise in robotic environments, which often leads to fragmented structural anchors.

**Table 8. Ablation Study on Edge Detection Operators.** We evaluate the impact of various geometric priors on manipulation success rates and latency. The Sobel operator is selected for its superior balance of physical robustness and computational efficiency.

Method	Success Rate (%)				Latency	
	Spa.	Obj.	Goal	Long	Avg.	(ms)
OpenVLA-OFT (Base)	98.6	98.2	96.6	94.8	97.1	123.2
<i>Comparison with Traditional and DL-based Operators</i>						
VLA-IAP (Canny)	97.2	98.8	97.4	93.8	96.8	104.5
VLA-IAP (HED)	97.4	<b>99.6</b>	98.2	94.4	97.4	125.1
VLA-IAP (BDCN)	<b>97.6</b>	99.0	98.2	95.2	97.5	132.8
<b>VLA-IAP (Sobel)</b>	<b>97.6</b>	<b>99.6</b>	<b>98.4</b>	<b>95.6</b>	<b>97.8</b>	<b>98.6</b>

Our results demonstrate that the Sobel operator provides the optimal trade-off for VLA tasks. It achieves a state-of-the-art success rate of 97.8% while maintaining a remarkably low latency of 98.6 ms. The continuous gradient response of Sobel is more compatible with our patch-level token scoring than the binary output of Canny, and its negligible computational footprint compared to HED/BDCN ensures that the inference gains from visual pruning are not offset by the cost of prior construction. This confirms that for embodied VLA models, a lightweight, purely physical prior is superior to complex semantic-based alternatives.

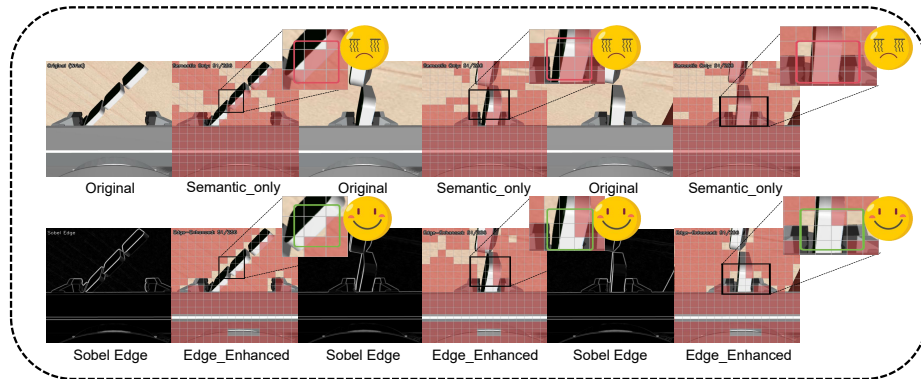


**Fig. 7. Visualization of the Geometric Prior (Edge Enhancement) on VLABench using  $\pi_{0.5}$ .** **Top:** The *Semantic-only* pruning strategy incorrectly discards structurally critical edge patches near the gripper-object interface (highlighted by red boxes), losing physical boundaries. **Bottom:** By incorporating the Sobel edge map (Geometric Prior), our *Edge-Enhanced* strategy successfully preserves these vital structural anchors (highlighted by green boxes), ensuring geometric continuity for precise robotic manipulation.

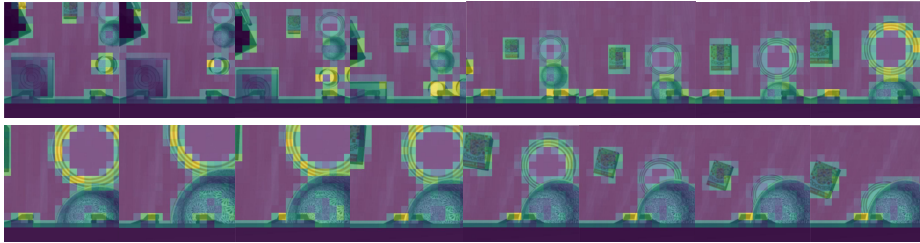


**Fig. 8. Geometric prior visualization on LIBERO (Wrist View).** The Sobel operator consistently extracts structural anchors of the target bowl and environmental constraints. These stable physical contours provide indispensable spatial references for fine manipulation, ensuring the retention of interaction-critical patches independent of the model’s semantic attention.

## B.6 More Visualization

**Qualitative Analysis of Edge Enhancement.** To further illustrate the efficacy of our proposed Geometric Prior, we provide a qualitative comparison on the VLABench using the  $\pi_{0.5}$  backbone. Fig. 7 focuses specifically on the wrist camera perspective during a fine manipulation phase.

When relying solely on semantic attention (Fig. 7, Top Row), the pruning mechanism frequently suffers from premature token dropping around structurally critical regions. Because physical boundaries and smooth edges inherently possess lower semantic saliency compared to textured backgrounds or the center of target objects, the *Semantic-only* strategy mistakenly discards these visually sparse patches. As highlighted by the red bounding boxes, the edges of the object being manipulated are heavily pruned. This loss of local geometric continuity deprives the VLA model of precise spatial and physical references precisely when the gripper interacts with the target.

In contrast, by integrating the Sobel-based Geometric Prior (Fig. 7, Bottom Row), our method explicitly extracts high-frequency physical contours independent of the VLM’s semantic space. As a result, the *Edge-Enhanced* strategy successfully forces the retention of these critical boundary patches (highlighted by the green bounding boxes). These preserved structural anchors guarantee that the policy maintains fine-grained spatial awareness, thereby preventing the catastrophic manipulation failures observed under extreme token compression.

**Qualitative Analysis of Geometric Priors.** As illustrated in Fig. 8, we visualize the extraction of geometric priors in the wrist-mounted camera sequence for a LIBERO task, sampling every 5 frames from frame 0 to 75. The Sobel operator consistently captures the high-frequency boundaries of the target black bowl and its environmental constraints, providing stable structural anchors essential for fine manipulation.

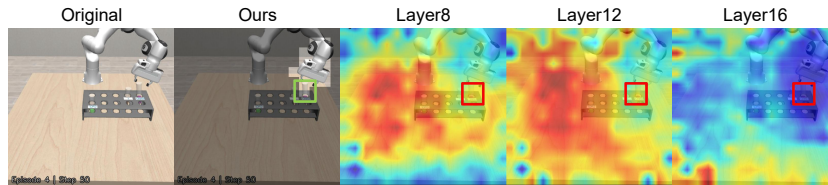


**Fig. 9. Visual analysis of LLM attention and aligned pruning on VLABench.** Heatmaps of  $\pi_{0.5}$ 's internal attention across layers (8, 12, 16) show the LLM focuses on irrelevant backgrounds instead of target objects due to limited fine-tuning on complex tasks.

**Failure Analysis of Attention-Guided Pruning.** To further investigate why perception-first baselines suffer from performance collapse on VLABench, we visualize the internal attention maps of the  $\pi_{0.5}$  backbone across multiple layers in Fig. 9. It is observed that due to the limited fine-tuning efficacy on such challenging manipulation tasks, the LLM fails to establish reliable grounding, with its attention predominantly focused on irrelevant background regions rather than the target objects. Consequently, pruning strategies that solely rely on these internal attention signals (such as FastV and SparseVLM) inevitably discard critical task-relevant tokens, leading to the catastrophic failures reported in Table 7. In contrast, our VLA-IAP remains robust to the sub-optimal grounding of the backbone. By bypassing the unreliable internal attention maps and instead utilizing explicit interaction alignment and geometric priors, our method ensures that the critical objects are preserved even under aggressive pruning ratios. This visualization confirms that VLA-IAP achieves a superior balance between efficiency and task performance by decoupling the pruning process from the model's internal fine-tuning quality.

## References

1. Alvar, S.R., Singh, G., Akbari, M., Zhang, Y.: Divprune: Diversity-based visual token pruning for large multimodal models. In: Proceedings of the Computer Vision and Pattern Recognition Conference. pp. 9392–9401 (2025)
2. Black, K., Brown, N., Driess, D., Esmail, A., Equi, M., Finn, C., Fusai, N., Groom, L., Hausman, K., Ichter, B., et al.:  $\pi_0$ : A vision-language-action flow model for general robot control. arXiv preprint arXiv:2410.24164 (2024)
3. Brohan, A., Brown, N., Carbajal, J., Chebotar, Y., Dabis, J., Finn, C., Gopalakrishnan, K., Hausman, K., Herzog, A., Hsu, J., et al.: Rt-1: Robotics transformer for real-world control at scale. arXiv preprint arXiv:2212.06817 (2022)
4. Cen, J., Yu, C., Yuan, H., Jiang, Y., Huang, S., Guo, J., Li, X., Song, Y., Luo, H., Wang, F., et al.: Worldvla: Towards autoregressive action world model. arXiv preprint arXiv:2506.21539 (2025)
5. Chen, L., Zhao, H., Liu, T., Bai, S., Lin, J., Zhou, C., Chang, B.: An image is worth 1/2 tokens after layer 2: Plug-and-play inference acceleration for large vision-language models. In: European Conference on Computer Vision. pp. 19–35. Springer (2024)

6. Ding, L., Goshtasby, A.: On the canny edge detector. *Pattern recognition* **34**(3), 721–725 (2001)
7. He, J., Zhang, S., Yang, M., Shan, Y., Huang, T.: Bi-directional cascade network for perceptual edge detection. In: *Proceedings of the IEEE/CVF conference on computer vision and pattern recognition*. pp. 3828–3837 (2019)
8. Hong, K., Dai, G., Xu, J., Mao, Q., Li, X., Liu, J., Chen, K., Dong, Y., Wang, Y.: Flashdecoding++: Faster large language model inference on gpus. *arXiv preprint arXiv:2311.01282* (2023)
9. Hung, C.Y., Sun, Q., Hong, P., Zadeh, A., Li, C., Tan, U., Majumder, N., Poria, S., et al.: Nora: A small open-sourced generalist vision language action model for embodied tasks. *arXiv preprint arXiv:2504.19854* (2025)
10. Intelligence, P., Black, K., Brown, N., Darpinian, J., Dhabalia, K., Driess, D., Esmail, A., Equi, M., Finn, C., Fusai, N., et al.: pi0.5: a vision-language-action model with open-world generalization. *arXiv preprint arXiv:2504.16054* (2025)
11. Kim, M.J., Finn, C., Liang, P.: Fine-tuning vision-language-action models: Optimizing speed and success. *arXiv preprint arXiv:2502.19645* (2025)
12. Kim, M.J., Pertsch, K., Karamcheti, S., Xiao, T., Balakrishna, A., Nair, S., Rafailov, R., Foster, E., Lam, G., Sanketi, P., et al.: Openvla: An open-source vision-language-action model. *arXiv preprint arXiv:2406.09246* (2024)
13. Li, Q., Liang, Y., Wang, Z., Luo, L., Chen, X., Liao, M., Wei, F., Deng, Y., Xu, S., Zhang, Y., et al.: Cogact: A foundational vision-language-action model for synergizing cognition and action in robotic manipulation. *arXiv preprint arXiv:2411.19650* (2024)
14. Li, Y., Meng, Y., Sun, Z., Ji, K., Tang, C., Fan, J., Ma, X., Xia, S., Wang, Z., Zhu, W.: Sp-vla: A joint model scheduling and token pruning approach for vla model acceleration. *arXiv preprint arXiv:2506.12723* (2025)
15. Liu, B., Zhu, Y., Gao, C., Feng, Y., Liu, Q., Zhu, Y., Stone, P.: Libero: Benchmarking knowledge transfer for lifelong robot learning. *Advances in Neural Information Processing Systems* **36**, 44776–44791 (2023)
16. Mees, O., Hermann, L., Rosete-Beas, E., Burgard, W.: Calvin: A benchmark for language-conditioned policy learning for long-horizon robot manipulation tasks. *IEEE Robotics and Automation Letters* **7**(3), 7327–7334 (2022)
17. Pei, X., Chen, Y., Xu, S., Wang, Y., Shi, Y., Xu, C.: Action-aware dynamic pruning for efficient vision-language-action manipulation. *arXiv preprint arXiv:2509.22093* (2025)
18. Shukor, M., Aubakirova, D., Capuano, F., Kooijmans, P., Palma, S., Zouitine, A., Aractingi, M., Pascal, C., Russi, M., Marafioti, A., et al.: Smolvla: A vision-language-action model for affordable and efficient robotics. *arXiv preprint arXiv:2506.01844* (2025)
19. Wang, H., Xu, J., Pan, J., Zhou, Y., Dai, G.: Specprune-vla: Accelerating vision-language-action models via action-aware self-speculative pruning. *arXiv preprint arXiv:2509.05614* (2025)
20. Xie, S., Tu, Z.: Holistically-nested edge detection. In: *Proceedings of the IEEE international conference on computer vision*. pp. 1395–1403 (2015)
21. Xu, S., Wang, Y., Xia, C., Zhu, D., Huang, T., Xu, C.: Vla-cache: Towards efficient vision-language-action model via adaptive token caching in robotic manipulation. *arXiv e-prints* pp. arXiv–2502 (2025)
22. Yang, Y., Wang, Y., Wen, Z., Zhongwei, L., Zou, C., Zhang, Z., Wen, C., Zhang, L.: Efficientvla: Training-free acceleration and compression for vision-language-action models. *arXiv preprint arXiv:2506.10100* (2025)

23. Ye, Y., Ma, J., Cen, J., Lu, Z.: Token expand-merge: Training-free token compression for vision-language-action models. arXiv preprint arXiv:2512.09927 (2025)
24. Zhang, S., Xu, Z., Liu, P., Yu, X., Li, Y., Gao, Q., Fei, Z., Yin, Z., Wu, Z., Jiang, Y.G., et al.: Vlabench: A large-scale benchmark for language-conditioned robotics manipulation with long-horizon reasoning tasks. In: Proceedings of the IEEE/CVF International Conference on Computer Vision. pp. 11142–11152 (2025)
25. Zhang, W., Liu, H., Qi, Z., Wang, Y., Yu, X., Zhang, J., Dong, R., He, J., Lu, F., Wang, H., et al.: Dreamvla: a vision-language-action model dreamed with comprehensive world knowledge. arXiv preprint arXiv:2507.04447 (2025)
26. Zhang, Y., Fan, C.K., Ma, J., Zheng, W., Huang, T., Cheng, K., Gudovskiy, D., Okuno, T., Nakata, Y., Keutzer, K., et al.: Sparsevlm: Visual token sparsification for efficient vision-language model inference. arXiv preprint arXiv:2410.04417 (2024)
27. Zitkovich, B., Yu, T., Xu, S., Xu, P., Xiao, T., Xia, F., Wu, J., Wohlhart, P., Welker, S., Wahid, A., et al.: Rt-2: Vision-language-action models transfer web knowledge to robotic control. In: Conference on Robot Learning. pp. 2165–2183. PMLR (2023)